International Journal of Bifurcation and Chaos, Vol. 21, No. 4 (2011) 1099–1111

DOI: 10.1142/S0218127411029033

INFERRING INDIRECT COUPLING BY MEANS OF RECURRENCES

Y. ZOU[*,¶], M. C. ROMANO[†,‡], M. THIEL[†],
N. MARWAN[*] and J. KURTHS[*,†,§]
[*]*Potsdam Institute for Climate Impact Research, P. O. Box 60 12 03, 14412 Potsdam, Germany*
[†]*Institute for Complex Systems and Mathematical Biology, University of Aberdeen, Aberdeen AB24 3UE, United Kingdom*
[‡]*Institute of Medical Sciences, Foresterhill, University of Aberdeen, Aberdeen AB25 2ZD, United Kingdom*
[§]*Department of Physics, Humboldt University, Newtonstr. 15, 12489 Berlin, Germany*
[¶]*Yong.Zou@pik-potsdam.de*

Received March 8, 2010; Revised April 23, 2010

The identification of the coupling direction from measured time series taking place in a group of interacting components is an important challenge for many experimental studies. We propose here a method to uncover the coupling configuration using recurrence properties. The approach hinges on a generalization of conditional probability of recurrence, which was originally introduced to detect and quantify even weak coupling directions between two interacting systems, to the case of multivariate time series where indirect interactions might be present. We test our method by an example of three coupled Lorenz systems. Our results confirm that the proposed method has much potential to identify indirect coupling, which is very relevant for experimental time series analysis.

Keywords: Coupling direction; recurrences; Lorenz system; multivariate time series.

1. Introduction

The extraction of interaction information from measured time series is an important challenge in modern nonlinear sciences. The main issue is to unravel the governing functional interactions between subsystems contained in a large network. In most cases, a network has a complex topology of connectivity with many interacting subsystems [Albert & Barabasi, 2002; Boccaletti *et al.*, 2006]. Therefore, the process of identifying the network topology of interactions of such networks is crucial in understanding the mechanism of functional topology, for instance, in brain dynamics [Zhou *et al.*, 2006], maternal-fetal cardiac systems [Van Leeuwen *et al.*, 2009] and in climatological tele-connections [Tsonis & Swanson, 2008; Donges *et al.*, 2009a]. However, the correct extraction of connectivity from time series remains a nontrivial task.

One popular technique applied in the literature, for instance, in complex climate networks analysis, is the calculation of cross correlation coefficients of the time series for every pair of nodes [Yamasaki *et al.*, 2008; Tsonis & Swanson, 2008]. However, this method has been proved to be a rather rough estimation of the coupling strength and in many

systems, one needs methods taking into account nonlinear effects [Donges *et al.*, 2009a, 2009b]. More advanced methods taking into consideration nonlinear dependencies between the different nodes are often applicable to two or three nodes. Nevertheless, they constitute the first step in a more thorough analysis of the connectivity structure of a large network. Inferring the coupling configuration at a local scale can be of substantial help to explain the global functioning of the network, e.g. the finding of motifs can be crucial for the understanding of the whole system [Alon, 2006; Sporns & Kötter, 2004]. Therefore, in this paper, we focus on the inference of the coupling configuration of small networks consisting of three nodes.

The understanding of a driver-response relationship was firstly evaluated in a linear framework by bivariate autoregressive models, by means of Granger causality [Granger, 1969]. This has been mainly applied to economy and neurosciences [Ding *et al.*, 2007]. From the nonlinear perspective, there are four major approaches in the literature to address drive-response relationships: state-space based methods [Quiroga *et al.*, 2000], information theory based methods [Paluš & Vejmelka, 2007; Schreiber, 2000; Vejmelka & Paluš, 2008], phase dynamics based methods [Rosenblum & Pikovsky, 2001; Rosenblum *et al.*, 2002], and recurrence-based methods [Romano *et al.*, 2007; Nawrath *et al.*, 2010]. The state-space based approach hinges on the assumption of the existence of a smooth map between the driver X and the response system Y, as such close states of the driver X imply close states in the response of Y. In this spirit, several methods have been proposed by utilizing properties of nearest neighbors, such as cross predictability and relative average distance of mutual nearest neighbors [Quiroga *et al.*, 2000]. However, this approach is usually system-dependent, but fails to yield the correct coupling in paradigmatic examples as in two chaotic Rössler systems [Paluš & Vejmelka, 2007].

The methods based on information theory need to calculate the information contained in each subsystem and quantify the net influence (e.g. transfer information) flow from one system X to the other system Y. Several applicable algorithms have been proposed to estimate the transfer information flow [Schreiber, 2000]. Recent developments in calculating transfer information use order patterns of time series, yielding symbolic transfer entropy or permutation information [Bahraminasab *et al.*, 2008; Staniek & Lehnertz, 2008]. However, these techniques are currently aimed at bivariate situations. Only recently this method has been extended to deal with multivariate cases [Frenzel & Pompe, 2007].

Phase dynamics-based methods estimate the phase components as a first step, but it is not always possible to assign a phase to a system, in particular, if the power spectrum does not show a pronounced frequency peak (i.e. nonphase-coherent case). A systematic comparison of methods based on phase dynamics and state-space was carried out in [Smirnov & Andrzejak, 2005], where the authors concluded that neither of the methods is better than the other one. Moreover, some spurious dependencies could be identified for real time series analysis [Osterhage *et al.*, 2008].

Recently, Romano *et al.* [2007] introduced a new method to detect and quantify the asymmetry of the coupling between two interacting systems based on their recurrence properties. This method successfully detects the direction of the coupling even in weakly as well as structurally different systems. The main idea hinges on the asymmetry of the complexity between the driving system X and the driven system Y. We will shortly review this technique in Sec. 3. Originally, it has focused on bivariate situations. It is crucial to extend it to multivariate time series analysis as this occurs quite often in many real applications.

Let us start considering the following small network as in Fig. 1, showing six different coupling settings for three unidirectionally interacting nodes.

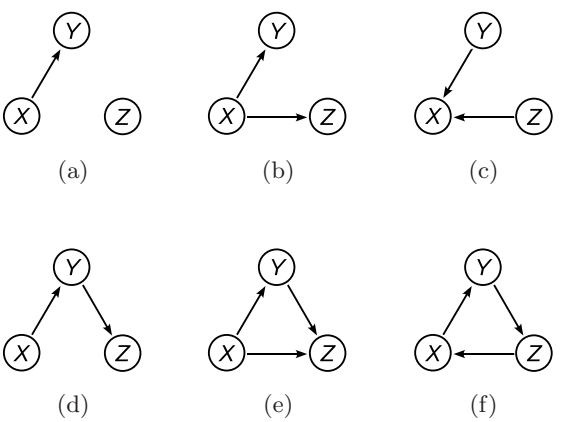

Fig. 1. Coupling configuration settings for three systems, that only unidirectional couplings are considered. (a) Z is independent of both X and Y. (b) X is the common driver for both Y and Z. (c) X is coregulated by Y and Z. (d) X drives Y, while Y further drives Z. (e) Direct coupling with X being the common driver and Z being the common response. (f) Direct coupling in a ring way.

A pairwise analysis (bivariate) is often insufficient in addressing the possible indirect coupling [e.g. the coupling between X and Z in Fig. 1(d)]. Hence, one main objective of this paper is to identify the indirect coupling by recurrences. More specifically, we will identify the difference among these six coupling cases by studying the recurrence properties. The advantage of the extension from two to three coupled systems is that it makes possible to analyze data measured from small networks, such as the EEG recordings on the scalp, so frequently used in neuroscience and cognitive psychology. In such experimental situations we have access to time series from typically of the order of 10 nodes. Furthermore, it is crucial to identify the indirect coupling between X and Z as illustrated by Fig. 1(d) since it is one of the big challenges for multivariate analysis. Therefore, we extend the study of Romano *et al.* [2007] to three oscillators.

We show numerical studies for the application to three coupled Lorenz systems with six different coupling configurations (Fig. 1). Specifically, we consider the following system

$$X: \begin{cases} \dot{x}_1 = \sigma(x_2 - x_1), \\ \dot{x}_2 = rx_1 - x_2 - x_1x_3 + \mu_{21}y_2^2 + \mu_{31}z_3^2, \\ \dot{x}_3 = x_1x_2 - bx_3, \end{cases} \quad (1)$$

$$Y: \begin{cases} \dot{y}_1 = \sigma(y_2 - y_1), \\ \dot{y}_2 = ry_1 - y_2 - y_1y_3 + \mu_{12}x_2^2 + \mu_{32}z_3^2, \\ \dot{y}_3 = y_1y_2 - by_3, \end{cases} \quad (2)$$

$$Z: \begin{cases} \dot{z}_1 = \sigma(z_2 - z_1), \\ \dot{z}_2 = rz_1 - z_2 - z_1z_3 + \mu_{13}x_2^2 + \mu_{23}y_2^2, \\ \dot{z}_3 = z_1z_2 - bz_3. \end{cases} \quad (3)$$

We integrate these equations numerically by a fourth order Runge–Kutta method of step 0.003 but with sampling every 100th point leading to time step $\Delta t = 0.3$. We use standard parameters $\sigma = 10, r = 28, b = 8/3$ as in the uncoupled case $\mu_{i,j} = 0$ so that the oscillators are in a chaotic regime.

Our procedure to deal with the six coupling settings of Fig. 1 has three steps, which are explained in different sections: in Sec. 2, we apply a univariate analysis, namely analyzing each individual system separately; in Sec. 3, we perform a pairwise analysis, after which only the coupling configuration of Figs. 1(d) and 1(e) remains unclear. In Sec. 4, the partial mean conditional probability of recurrence is developed to cope with the last two remaining cases. Some conclusions are drawn in Sec. 6.

2. First Step: Univariate Analysis

Our method hinges on one fundamental tool for nonlinear time series analysis, namely, recurrence plots (RPs). Given a trajectory of a dynamical system consisting of different values $\mathbf{x}_i$, i.e. a sampled trajectory from system X, where i indicates the time of observation, the corresponding RP is defined as [Eckmann *et al.*, 1987; Marwan *et al.*, 2007]

$$R_{i,j}(\varepsilon) = \Theta(\varepsilon - \|\mathbf{x}_i - \mathbf{x}_j\|), \quad (4)$$

where $\Theta(\cdot)$ is the Heaviside function, $\|\cdot\|$ is the distance between two observations in phase space (which will be measured in terms of the maximum norm from now on because of computational efficiency), and ε a predefined threshold for the proximity of two states in phase space, i.e. for distinguishing whether or not two observations are neighbors in phase space. By visualizing this matrix with black ($R_{i,j} = 1$) and white ($R_{i,j} = 0$) dots, different types of dynamics can be identified in terms of different types of line structures (including single points, blocks, and extended diagonal or vertical lines), which can be quantitatively assessed in terms of the recurrence quantification analysis [Marwan *et al.*, 2007].

Here we are particularly interested in the mean probability of recurrence (recurrence rate), which is estimated by

$$\langle p(x_j)\rangle = \mathrm{RR} = \frac{1}{N^2}\sum_{i,j=1}^{N} R_{i,j}. \quad (5)$$

The first step is to study the variations of the mean probability of recurrences with respect to an increase of the coupling strength (Fig. 1), separately. For instance, in the case of coupling as in Fig. 1(a), both $\langle p(x)\rangle$ and $\langle p(z)\rangle$ remain unchanged while $\langle p(y)\rangle$ varies if the coupling strength μ is

Table 1. Variation of RR of each individual system. The symbols "+" correspond to the existence of variation, while "−" means there are no changes with increase of coupling strength.

	(a)	(b)	(c)	(d)	(e)	(f)
RR_X	−	−	+	−	−	+
RR_Y	+	+	−	+	+	+
RR_Z	−	+	−	+	+	+

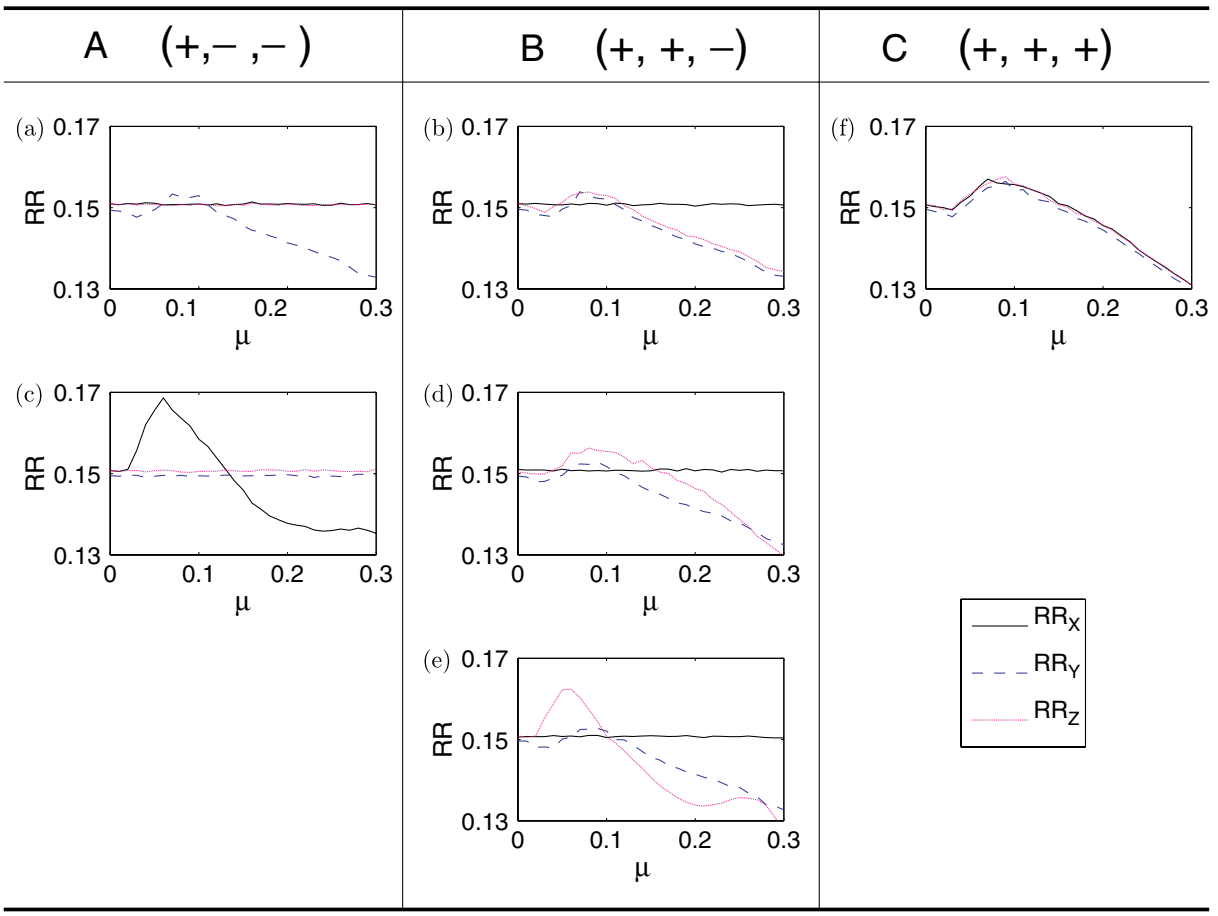

Fig. 2. Univariate analysis. Six coupling cases are classified into three groups A, B and C according to our univariate analysis.

increased. This is because Z is independent of X and Y and the coupling from X to Y is unidirectional. A similar analysis can be achieved for each coupling setting of Fig. 1. We summarize the result in Table 1. We note that, throughout the paper, the symbols "+" correspond to a change of the recurrence rate of the component, while "−" means there are no changes with increase of the coupling strength. Furthermore "(a), . . . , (f)" denote the six different coupling configurations, as shown in Fig. 1.

The numerical simulation for the first step is shown in Fig. 2, which verifies the results presented in Table 1. By the first step of the univariate analysis, six different couplings are subdivided into three categories: $(+,-,-)$, $(+,+,-)$, and $(+,+,+)$. Note that $(+,-,-)$ denotes the configurations for which only the RR of one component changes with the coupling strength no matter which component. Therefore, the coupling configurations (a) and (c) are classified in the same group A.

Note that in principle one could also use other measures from Recurrence Quantification Analysis (RQA) [Marwan *et al.*, 2007] for this first step analysis. However it is not clear whether their use would allow identifying the coupling configuration. Moreover, the interpretation of the results might be difficult and rather empirical. Nevertheless, it is important to note that the probability of recurrence has a deep theoretical meaning as it is the basis for calculating many dynamical invariants, i.e. correlation dimension D_2 [Grassberger & Procaccia, 1983]. Furthermore, it has a clear relationship with information theoretic approaches (see [Paluš & Vejmelka, 2007]).

3. Second Step: Pairwise Analysis

In the second step, we perform a pairwise analysis, which was first introduced in [Romano *et al.*, 2007]. This method is based on a generalization of the RPs to joint recurrence plots (JRPs), capturing

the interplay between two dynamical systems. JRP is calculated by

$$\mathbf{JRP}_{i,j}^{X,Y} = \Theta(\varepsilon_X - \|\mathbf{x}_i - \mathbf{x}_j\|) \times \Theta(\varepsilon_Y - \|\mathbf{y}_i - \mathbf{y}_j\|), \quad i,j = 1,\ldots,N. \tag{6}$$

The extension to three interacting systems can be made in full analogy.

In order to identify the coupling direction, one needs to consider the mean conditional probabilities of recurrence (MCR) of systems X and Y, which are defined as follows:

$$\mathrm{MCR}(Y \,|\, X) = \frac{1}{N}\sum_{j=1}^{N} p(\mathbf{y}_j \,|\, \mathbf{x}_j) = \frac{1}{N}\sum_{j=1}^{N} \frac{\sum_{i=1}^{N} JR_{i,j}^{X,Y}}{\sum_{i=1}^{N} R_{i,j}^{X}} \tag{7}$$

and

$$\mathrm{MCR}(X \,|\, Y) = \frac{1}{N}\sum_{j=1}^{N} p(\mathbf{x}_j \,|\, \mathbf{y}_j) = \frac{1}{N}\sum_{j=1}^{N} \frac{\sum_{i=1}^{N} JR_{i,j}^{X,Y}}{\sum_{i=1}^{N} R_{i,j}^{Y}}, \tag{8}$$

where $p(\mathbf{y}_j \,|\, \mathbf{x}_j)$ is an estimation of the probability that the trajectory of Y recurs to the neighborhood of $\mathbf{y}_j$ under the condition that the trajectory of X recurs to the neighborhood of $\mathbf{x}_j$. In the presence of the asymmetry of the coupling (e.g. suppose X to be driver and Y to be response without the loss of generality), we have the following relationship

$$\mathrm{MCR}(Y \,|\, X) < \mathrm{MCR}(X \,|\, Y). \tag{9}$$

The interpretation of the inequality (9) is based on the difference of complexity between X and Y. If X drives Y, the dimension of Y will be larger than the dimension of X because the dynamics of Y is determined by both the states of X and Y, while Y does not influence X. Note that this only holds provided the coupling strength is smaller than the threshold for synchronization, as the coupling direction might be lost if both systems become completely synchronized. Increasing the coupling strength from X to Y, the complexity of Y increases. This results in a decrease of the recurrence probability $p(\mathbf{y}_j)$ that Y recurs to the neighborhood. However, the complexity of X remains constant with increasing coupling strength because X is independent of Y (not vice versa). Hence, the mean recurrence probability of $\langle p(\mathbf{x}_j)\rangle > \langle p(\mathbf{y}_j)\rangle$, implying $\sum_{i=1}^{N} R_{i,j}^{X} > \sum_{i=1}^{N} R_{i,j}^{Y}$. Therefore, we have $\mathrm{MCR}(Y \,|\, X) < \mathrm{MCR}(X \,|\, Y)$ if X is the driver. For convenience, we calculate

$$\Delta\mathrm{MCR}(Y \,|\, X) = \mathrm{MCR}(Y \,|\, X) - \mathrm{MCR}(X \,|\, Y). \tag{10}$$

The existence of coupling is justified by the variation of $\Delta(Y \,|\, X)$, while the directionality (i.e. X is the driver) is determined by whether this value is negative, or vice versa, provided the coupling strength is systematically changed. The contribution of X to $\mathrm{MCR}(Y \,|\, X)$ tends to zero if it is independent of Y, namely we get

$$\mathrm{MCR}(Y \,|\, X) = \frac{1}{N}\sum_{j=1}^{N} p(\mathbf{y}_j \,|\, \mathbf{x}_j) = \frac{1}{N}\sum_{j=1}^{N} p(\mathbf{y}_j) = \mathrm{RR}_Y. \tag{11}$$

In other words, the condition that X recurs does not influence the recurrence probability of Y (the same holds for $\mathrm{MCR}(X \,|\, Y) = \mathrm{RR}_X$, if X and Y are independent).

Note that the numerator of Eq. (7) or (8) is related to the information dimension for a strange object (in this case, the object is the composition of X and Y in a joint phase space) [Ott, 1993]. For the subsystem X, $\sum_{i=1}^{N} R_{i,j}^{X}$ appearing as denominator of Eq. (7) is used to calculate the information dimension for system X. In this regard, $\mathrm{MCR}(Y \,|\, X)$ [Eq. (7)] is an average ratio between the pointwise dimension value of (X, Y) and the pointwise dimension value of X over the entire trajectory.

Based on the results obtained in the first step (Table 1 and Fig. 6), we do the pairwise analysis for cases A and B, following the notation of Fig. 2 since in case C we have only one coupling configuration. Furthermore, we characterize the results of the pairwise analysis using the same notations as before. For instance, if $\Delta\mathrm{MCR}(X \,|\, Y)$ changes with

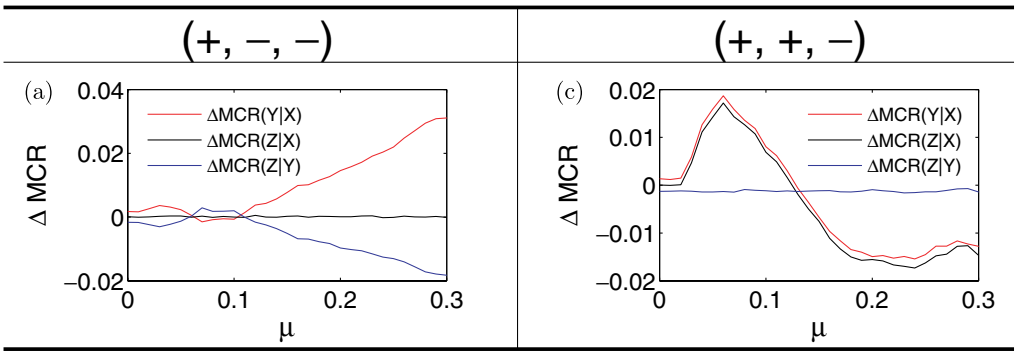

Fig. 3. Pairwise comparison for coupling (a, c). The left panel is for coupling configuration (a), the right panel is for coupling configuration (c). Note that in (a), $\Delta\mathrm{MCR}(Z\,|\,Y)$ is completely overlapped with the difference between RR_Y and RR_Z, which can be obtained from the first step of the univariate analysis (see Fig. 2).

the coupling strength whereas $\Delta\mathrm{MCR}(X\,|\,Z)$ and $\Delta\mathrm{MCR}(Y\,|\,Z)$ stay constant, we write $(+,-,-)$. In particular, we have explicit expressions for Eq. (10) for each coupling:

(A) couplings (a) and (c)

(a) $(+,-,-)$

$$\begin{aligned}&\Delta\mathrm{MCR}(Y\,|\,X) > 0,\\ &\Delta\mathrm{MCR}(Z\,|\,X) = \mathrm{RR}_Z - \mathrm{RR}_X \approx 0,\\ &\Delta\mathrm{MCR}(Z\,|\,Y) = \mathrm{RR}_Y - \mathrm{RR}_Z.\end{aligned} \tag{12}$$

Note that RR_Y changes with the coupling strength, leading to $\Delta\mathrm{MCR}(Z\,|\,Y) < 0$. However, $\Delta\mathrm{MCR}(Z\,|\,Y)$ simply follows the same curve of univariate analysis since Y is independent of Z. In this respect, we denote it as "–".

(c) $(+,+,-)$

$$\begin{aligned}&\Delta\mathrm{MCR}(Y\,|\,X) < 0,\\ &\Delta\mathrm{MCR}(Z\,|\,X) < 0,\\ &\Delta\mathrm{MCR}(Z\,|\,Y) = \mathrm{RR}_Z - \mathrm{RR}_Y \approx 0.\end{aligned} \tag{13}$$

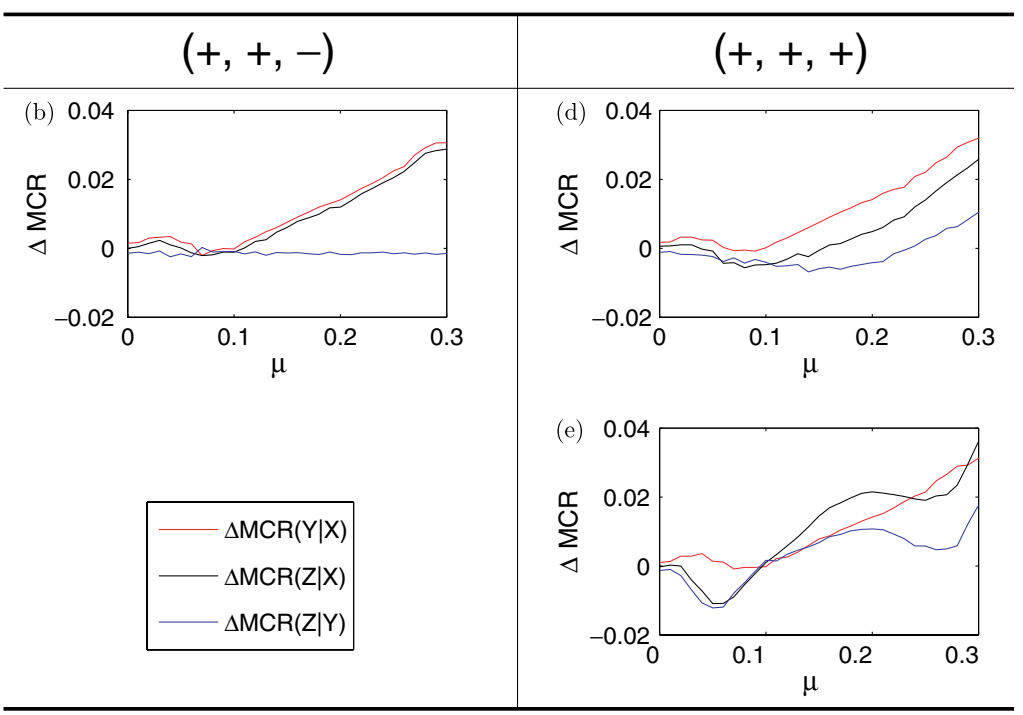

Fig. 4. Pairwise comparison for coupling configurations (b, d, e). The left panel is for (b), the right panel is for coupling configurations (d, e).

(B) couplings (b), (d) and (e)

(b) $(+,+,-)$

$$\begin{aligned}\Delta\mathrm{MCR}(Y\,|\,X) &> 0,\\ \Delta\mathrm{MCR}(Z\,|\,X) &> 0,\\ \Delta\mathrm{MCR}(Z\,|\,Y) &\approx 0.\end{aligned} \tag{14}$$

(d, e) $(+,+,+)$

$$\begin{aligned}\Delta\mathrm{MCR}(Y\,|\,X) &> 0,\\ \Delta\mathrm{MCR}(Z\,|\,X) &> 0,\\ \Delta\mathrm{MCR}(Z\,|\,Y) &> 0.\end{aligned} \tag{15}$$

Therefore, after the pairwise analysis, only cases (d) and (e) remain ambiguous.

The numerical simulations for the pairwise analysis of the second step are shown in Figs. 3(a), 3(c), 4(b), 4(d) and 4(e), respectively.

4. Third Step: Partial MCR

A recurrence-based bivariate analysis is generally not conclusive in addressing the existence of indirect coupling. Hence, we go to the crucial step in extending the method to deal with the remaining two coupling cases (d) and (e) after the previous two steps.

Let us first consider MCR of two variables used in our previous bivariate analysis, i.e. the pair of X and Y. We calculate $\mathrm{MCR}(Y\,|\,X)$ and $\mathrm{MCR}(X\,|\,Y)$, respectively. The second step is to quantify the influence of the third variable Z on $\mathrm{MCR}(Y\,|\,X)$ by considering the difference between $\mathrm{MCR}(Y\,|\,X)$ and the mean conditional probability of recurrence that Y recurs given that *both* X and Z recur,

$$\begin{aligned}&\Delta\mathrm{MCR}(Y\,|\,X)_Z\\ &\quad= -(\mathrm{MCR}(Y\,|\,X) - \mathrm{MCR}(Y\,|\,X,Z)).\end{aligned} \tag{16}$$

Similarly the contribution of Z to the $\mathrm{MCR}(X\,|\,Y)$ is calculated by

$$\begin{aligned}&\Delta\mathrm{MCR}(X\,|\,Y)_Z\\ &\quad= -(\mathrm{MCR}(X\,|\,Y) - \mathrm{MCR}(X\,|\,Y,Z)).\end{aligned} \tag{17}$$

Before synchronization sets in, we have MCR $(Y\,|\,X) < \mathrm{MCR}(Y\,|\,X,Z)$ due to $\langle p(\mathbf{x}_j)\rangle > \langle p(\mathbf{x}_j,\mathbf{z}_j)\rangle$. Hence, for convenience, the normalization factor (negative symbol) in front of the right-hand side in Eq. (16) is introduced to keep the probability values to be positive. Note that $\Delta\mathrm{MCR}(Y\,|\,X)_Z$ quantifies a subset of $\mathrm{MCR}(Y\,|\,X)$, measuring the contribution of Z to the probabilities of recurrence of Y via X. In this regard, we call $\Delta\mathrm{MCR}(Y\,|\,X)_Z$ *partial* MCR. Moreover, in general $\Delta\mathrm{MCR}(Y\,|\,X)_Z$ is different from $\Delta\mathrm{MCR}(X\,|\,Y)_Z$ because of the asymmetry between $\mathrm{MCR}(Y\,|\,X)$ and $\mathrm{MCR}(X\,|\,Y)$.

Analogously, the contribution of Y to MCR $(Z\,|\,X)$ and $\mathrm{MCR}(X\,|\,Z)$ is calculated, respectively, by

$$\begin{aligned}&\Delta\mathrm{MCR}(Z\,|\,X)_Y\\ &\quad= -(\mathrm{MCR}(Z\,|\,X) - \mathrm{MCR}(Z\,|\,X,Y)),\end{aligned} \tag{18}$$

$$\begin{aligned}&\Delta\mathrm{MCR}(X\,|\,Z)_Y\\ &\quad= -(\mathrm{MCR}(X\,|\,Z) - \mathrm{MCR}(X\,|\,Y,Z)).\end{aligned} \tag{19}$$

The contribution of X to $\mathrm{MCR}(Y\,|\,Z)$ and $\mathrm{MCR}(Z\,|\,Y)$ is computed by

$$\begin{aligned}&\Delta\mathrm{MCR}(Y\,|\,Z)_X\\ &\quad= -(\mathrm{MCR}(Y\,|\,Z) - \mathrm{MCR}(Y\,|\,X,Z)),\end{aligned} \tag{20}$$

$$\begin{aligned}&\Delta\mathrm{MCR}(Z\,|\,Y)_X\\ &\quad= -(\mathrm{MCR}(Z\,|\,Y) - \mathrm{MCR}(Z\,|\,X,Y)).\end{aligned} \tag{21}$$

Depending on the particular coupling configuration [Figs. 1(a)–1(f)], we obtain explicit expressions for measuring the contribution of one system to the other two. The details are presented in the Appendix. In this section, however, we focus on the remaining two coupling configurations that have still to be distinguished, namely (d) and (e).

(d) From the viewpoint of Z, the contribution of indirect coupling from X to Z is smaller than that of the direct coupling from Y to Z. Hence $\mathrm{MCR}(Z\,|\,X) < \mathrm{MCR}(Z\,|\,Y)$ and considering Eqs. (18) and (21) we have

$$\Delta\mathrm{MCR}(Z\,|\,Y)_X < \Delta\mathrm{MCR}(Z\,|\,X)_Y. \tag{22}$$

This is validated by showing a similar relationship from the X perspective, namely, $\mathrm{MCR}(X\,|\,Z) < \mathrm{MCR}(X\,|\,Y)$ implying

$$\Delta\mathrm{MCR}(X\,|\,Y)_Z < \Delta\mathrm{MCR}(X\,|\,Z)_Y. \tag{23}$$

However, from the mediator Y viewpoint, one has

$$\Delta\mathrm{MCR}(Y\,|\,X)_Z \lessapprox \Delta\mathrm{MCR}(Y\,|\,Z)_X, \tag{24}$$

indicating Y to be a mediator.

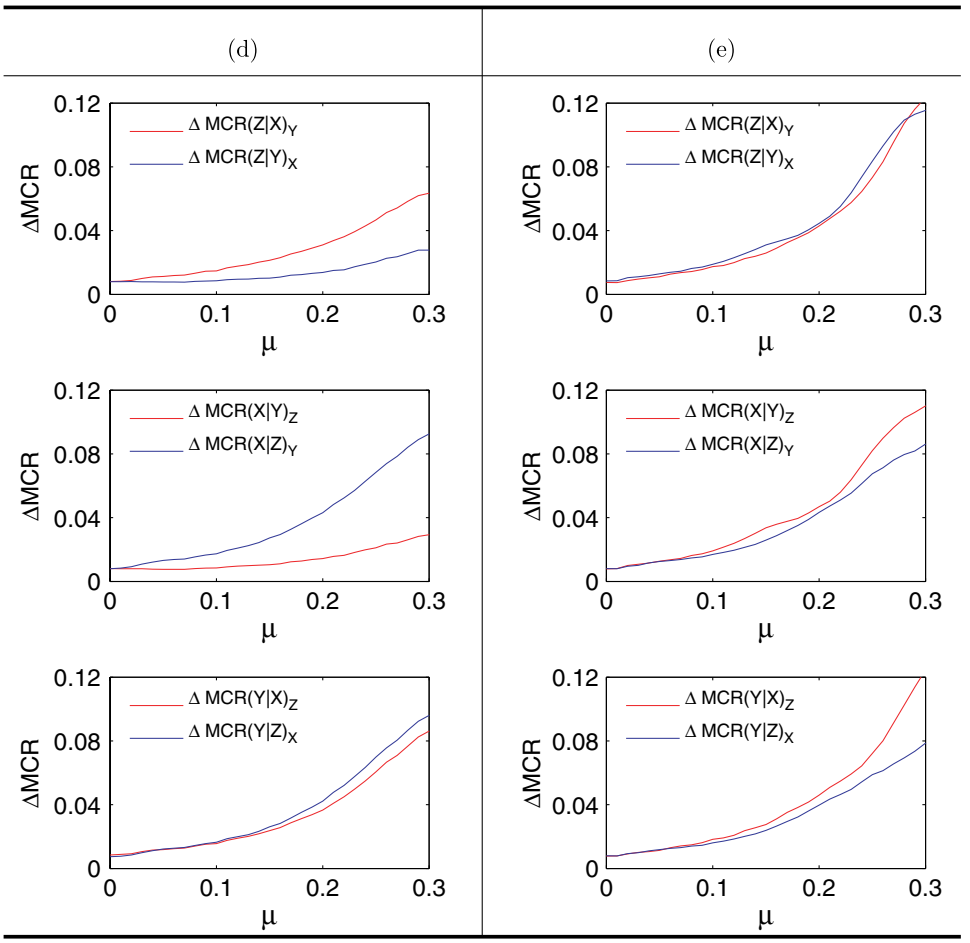

Fig. 5. Partial MCR shows distinct behavior for the coupling configurations (d) and (e).

(e) In this case, from the perspective of system Z, the contribution of X to Z is larger than the contribution of Y to Z, which implies $\mathrm{MCR}(Z\,|\,Y) < \mathrm{MCR}(Z\,|\,X)$. This yields, considering again Eqs. (18) and (21),

$$\Delta\mathrm{MCR}(Z\,|\,X)_Y < \Delta\mathrm{MCR}(Z\,|\,Y)_X. \quad (25)$$

This relationship is validated from the X perspective, $\mathrm{MCR}(X\,|\,Y) < \mathrm{MCR}(X\,|\,Z)$, implying

$$\Delta\mathrm{MCR}(X\,|\,Z)_Y < \Delta\mathrm{MCR}(X\,|\,Y)_Z. \quad (26)$$

Moreover, from the viewpoint of Y, we have

$$\Delta\mathrm{MCR}(Y\,|\,Z)_X < \Delta\mathrm{MCR}(Y\,|\,X)_Z. \quad (27)$$

The numerical simulations for the partial MCR analysis for the coupling configurations (d, e) involved in the third step are shown in Fig. 5, which agree with our theoretical expectation in a reasonable range for coupling strengths.

5. Decision Tree

Following the discussions presented in previous sections, we conclude that the six different coupling configurations are clearly identified with our three-step procedure (plotted as a decision tree in Fig. 6):

First: Univariate analysis, namely the probability of recurrences for each individual system, identifies the coupling configuration of (f). Note that couplings (a, c) are not able to be further classified because of the relabeling.

Second: Pairwise analysis, allows distinguishing the coupling configuration of (a) from (c), and (b) from (d, e).

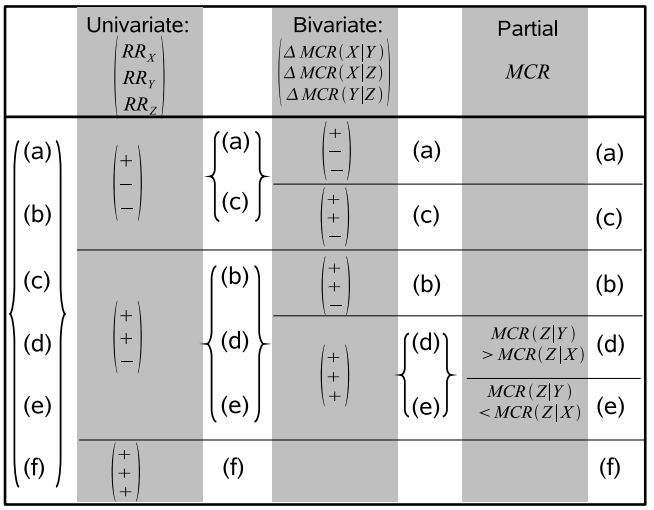

Fig. 6. Decision tree derived from the theoretical analysis. Our procedure consists of three steps, namely univariate, pairwise and partial MCR analysis.

Third: Partial MCR analysis identifies the difference between coupling (d) and (e).

6. Conclusions

We have proposed a new method to uncover the coupling structure of a small network, which hinges on the recurrence properties of the underlying systems. Due to the dimensional asymmetry between the driver and the response systems, the mean conditional recurrence probabilities of $\mathrm{MCR}(Y \,|\, X)$ and $\mathrm{MCR}(X \,|\, Y)$ are asymmetric. We have shown that a generalization to three coupled systems, in particular including the extraction of indirect coupling, is a challenging problem that can be tackled by considering the partial MCR. We have demonstrated our procedure using three Lorenz oscillators in chaotic regime in six different coupling configurations.

We plan to apply the proposed method to experimental data, e.g. climate time series in order to infer the coupling structure. This will be the subject of future research. Some issues might appear in this line of research, which have to be taken into consideration. Noise is ubiquitous in experimental time series and requires developing robust measures to identify the correct coupling configuration. It has been demonstrated that most recurrence structures are preserved if the free parameter ϵ [threshold in the recurrence matrix Eq. (4)] is chosen as $\epsilon \approx 5\sigma$, where σ corresponds to the standard deviation of the observational noise [Thiel *et al.*, 2002]. For the application to a large network of coupled units, the method has to be adapted to keep a good statistical power and to reduce the computation time. A further issue that will be considered in the future is the presence of asymmetric bidirectional coupling, as it is rather common in experimental complex networks.

Acknowledgments

This work has been financially supported by the German Research Foundation (SFB 555), the Potsdam Research Cluster for Georisk Analysis, Environmental Change and Sustainability (PROGRESS), the Leibniz association (project ECONS), the Scottish Universities Life Science Alliance (SULSA) and the RCUK academic fellowship from the EPSRC.

References

Albert, R. & Barabasi, A. L. [2002] "Statistical mechanics of complex networks," *Rev. Mod. Phys.* **74**.

Alon, U. [2006] *An Introduction to Systems Biology: Design Principles of Biological Circuits*, Chapman & Hall/CRC Mathematical & Computational Biology (Chapman & Hall).

Bahraminasab, A., Ghasemi, F., Stefanovska, A., McClintock, P. V. E. & Kantz, H. [2008] "Direction of coupling from phases of interacting oscillators: A permutation information approach," *Phys. Rev. Lett.* **100**, 084101.

Boccaletti, S., Latora, V., Moreno, Y., Chavez, M. & Hwang, D. U. [2006] "Complex networks: Structure and dynamics," *Phys. Rep.* **424**, 175–308.

Ding, M., Chen, Y. & Bressler, S. L. [2007] "Granger causality: Basic theory and application to neuroscience," *Handbook of Time Series Analysis*, eds. Schelter, B., Winterhalder, M. & Timmer, J. (Wiley-VCH Verlag GmbH & Co. KGaA), pp. 437–460.

Donges, J., Zou, Y., Marwan, N. & Kurths, J. [2009a] "The backbone of the climate network," *Europhys. Lett.* **87**, 48007.

Donges, J. F., Zou, Y., Marwan, N. & Kurths, J. [2009b] "Complex networks in climate dynamics — Comparing linear and nonlinear network construction methods," *Eur. Phys. J. ST* **174**, 157–179.

Eckmann, J.-P., Kamphorst, S. & Ruelle, D. [1987] "Recurrence plots of dynamical system," *Europhys. Lett.* **4**, 973–977.

Frenzel, S. & Pompe, B. [2007] "Partial mutual information for coupling analysis of multivariate time series," *Phys. Rev. Lett.* **99**, 204101.

Granger, C. W. J. [1969] "Investigating causal relations by econometric models and cross-spectral methods," *Econometrica* **37**, 424–438.
Grassberger, P. & Procaccia, I. [1983] "Characterization of strange attractor," *Phys. Rev. Lett.* **50**, 346–349.
Marwan, N., Romano, M., Thiel, M. & Kurths, J. [2007] "Recurrence plots for the analysis of complex systems," *Phys. Rep.* **438**, 237–329.
Nawrath, J., Romano, M. C., Thiel, M., Kiss, I. Z., Wickramasinghe, M., Timmer, J., Kurths, J. & Schelter, B. [2010] "Distinguishing direct from indirect interactions in oscillatory networks with multiple time scales," *Phys. Rev. Lett.* **104**, 038701.
Osterhage, H., Mormann, F., Wagner, T. & Lehnertz, K. [2008] "Detecting directional coupling in the human epileptic brain: Limitations and potential pitfalls," *Phys. Rev. E* **77**, 011914.
Ott, E. [1993] *Chaos in Dynamical Systems* (Cambridge University Press).
Paluš, M. & Vejmelka, M. [2007] "Directionality of coupling from bivariate time series: How to avoid false causalities and missed connections," *Phys. Rev. E* **75**, 056211.
Quiroga, R. Q., Arnhold, J. & Grassberger, P. [2000] "Learning driver-response relationships from synchronization patterns," *Phys. Rev. E* **61**, 5142–5148.
Romano, M. C., Thiel, M., Kurths, J. & Grebogi, C. [2007] "Estimation of the direction of the coupling by conditional probabilities of recurrence," *Phys. Rev. E* **76**, 036211.
Rosenblum, M. G. & Pikovsky, A. S. [2001] "Detecting direction of coupling in interacting oscillators," *Phys. Rev. E* **64**, 045202.
Rosenblum, M. G., Cimponeriu, L., Bezerianos, A., Patzak, A. & Mrowka, R. [2002] "Identification of coupling direction: Application to cardiorespiratory interaction," *Phys. Rev. E* **65**, 041909.
Schreiber, T. [2000] "Measuring information transfer," *Phys. Rev. Lett.* **85**, 461–464.
Smirnov, D. A. & Andrzejak, R. G. [2005] "Detection of weak directional coupling: Phase-dynamics approach versus state-space approach," *Phys. Rev. E* **71**, 036207.
Sporns, O. & Kötter, R. [2004] "Motifs in brain networks," *PLoS Biol.* **2**, e369.
Staniek, M. & Lehnertz, K. [2008] "Symbolic transfer entropy," *Phys. Rev. Lett.* **100**, 158101.
Thiel, M., Romano, M., Kurths, J., Meucci, R., Allaria, E. & Arecchi, F. [2002] "Influence of observational noise on the recurrence quantification analysis," *Physica D* **171**, 138–152.
Tsonis, A. A. & Swanson, K. L. [2008] "Topology and predictability of El Niño and La Niña networks," *Phys. Rev. Lett.* **100**, 228502.
Van Leeuwen, P., Geue, D., Thiel, M., Cysarz, D., Lange, S., Romano, M. C., Wessel, N., Kurths, J. & Grnemeyer, D. H. [2009] "Influence of paced maternal breathing on fetal maternal heart rate coordination," *Proc. Nat. Acad. Sci.* **106**, 13661–13666.
Vejmelka, M. & Paluš, M. [2008] "Inferring the directionality of coupling with conditional mutual information," *Phys. Rev. E* **77**, 026214.
Yamasaki, K., Gozolchiani, A. & Havlin, S. [2008] "Climate networks around the globe are significantly affected by El Niño," *Phys. Rev. Lett.* **100**, 228501.
Zhou, C. S., Zemanova, L., Zamora, G., Hilgetag, C. C. & Kurths, J. [2006] "Hierarchical organization unveiled by functional connectivity in complex brain networks," *Phys. Rev. Lett.* **97**, 238103.

Appendix

Partial MCR for all Couplings of Fig. 1

The detailed analysis for the partial MCR for the coupling settings of Fig. 1 is performed in this section. We assume that the three systems are identical in the case of zero coupling and that the coupling strengths can be changed systematically, which is often the case for many active experiments. Note that the numerical results are based on Eq. (1).

(a) Z independent of both X *and* Y [Fig. 1(a)]. We obtain $\mathrm{MCR}(Y \,|\, (X, Z)) = \mathrm{MCR}(Y \,|\, X)$. This means that the contribution of Z to $\mathrm{MCR}(Y \,|\, X)$ can be disregarded. Similarly, we have $\mathrm{MCR}(X \,|\, (Y, Z)) = \mathrm{MCR}(X \,|\, Y)$. Furthermore, $\mathrm{MCR}(Z \,|\, X) = \mathrm{RR}_Z$, $\mathrm{MCR}(Z \,|\, X, Y) = \mathrm{RR}_Z$, and $\mathrm{MCR}(Y \,|\, Z) = \mathrm{RR}_Y$ since Z is independent of both X and Y. Explicitly we have the following equations:

$$\Delta\mathrm{MCR}(X \,|\, Y)_Z = 0, \tag{A.1}$$

$$\Delta\mathrm{MCR}(X \,|\, Z)_Y = -(\mathrm{RR}_X - \mathrm{MCR}(X \,|\, Y)), \tag{A.2}$$

$$\Delta\mathrm{MCR}(Y \,|\, X)_Z = 0, \tag{A.3}$$

$$\Delta\mathrm{MCR}(Y \,|\, Z)_X = -(\mathrm{RR}_Y - \mathrm{MCR}(Y \,|\, X)), \tag{A.4}$$

$$\Delta\mathrm{MCR}(Z \,|\, X)_Y = 0, \tag{A.5}$$

$$\Delta\mathrm{MCR}(Z \,|\, Y)_X = 0. \tag{A.6}$$

In general Eqs. (A.2) and (A.4) are not equal because of the asymmetry between X and Y. Figure 7 shows the numerical result.

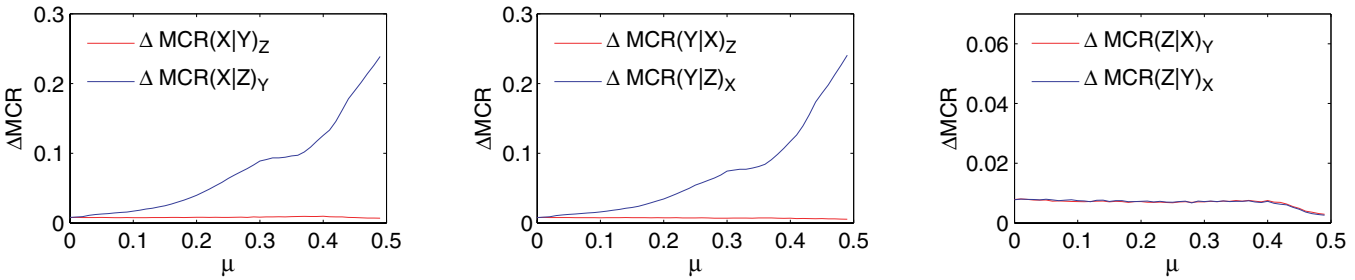

(a) (b) (c)

Fig. 7. Z is independent of both X and Y [Fig. 1(a), $\mu_{12} = \mu, \mu_{ij} = 0$ otherwise]. (a) From the viewpoint of X, $\Delta\mathrm{MCR}(X \,|\, Y) = 0$, [Eq. (A.1)]. (b) $\Delta\mathrm{MCR}(Y \,|\, X)_Z = 0$, [Eq. (A.3)]. However, due to the finite length of the time series used, these curves show some deviations from zero ($\mu = 0$). (c) $\Delta\mathrm{MCR}(Z \,|\, Y)_X \approx 0, \Delta\mathrm{MCR}(Z \,|\, X) \approx 0$.

(b) X is a common driver [Fig. 1(b)].
From the viewpoint of X, $\mathrm{MCR}(X \,|\, Y) = \mathrm{MCR}(X \,|\, Z)$, since Y and Z are identical. Hence we have

$$\Delta\mathrm{MCR}(X \,|\, Y)_Z = \Delta\mathrm{MCR}(X \,|\, Z)_Y. \quad \text{(A.7)}$$

It is also obvious to see that Y is independent of Z under the condition of X, yielding $\mathrm{MCR}(Y \,|\, Z) = \mathrm{RR}_Y$, $\mathrm{MCR}(Z \,|\, Y) = \mathrm{RR}_Z$, thus,

$$\Delta\mathrm{MCR}(Y \,|\, Z)_X = -(\mathrm{RR}_Y - \mathrm{MCR}(Y \,|\, X, Z)), \quad \text{(A.8)}$$

$$\Delta\mathrm{MCR}(Z \,|\, Y)_X = -(\mathrm{RR}_Z - \mathrm{MCR}(Z \,|\, X, Y)). \quad \text{(A.9)}$$

In general before reaching synchronization we have the mean recurrence probability relationship $\langle p(\mathbf{x}_j)\rangle > \langle p(\mathbf{y}_j)\rangle \approx \langle p(\mathbf{z}_j)\rangle$, $\langle p(\mathbf{x}_j, \mathbf{y}_j)\rangle > \langle p(\mathbf{y}_j, \mathbf{z}_j)\rangle = \langle p(\mathbf{y}_j)\rangle \cdot \langle p(\mathbf{z}_j)\rangle$. Hence, $\mathrm{MCR}(Y \,|\, X) > \mathrm{MCR}(Y \,|\, Z) = \mathrm{RR}_Y$, which leads to

$$\Delta\mathrm{MCR}(Y \,|\, X)_Z < \Delta\mathrm{MCR}(Y \,|\, Z)_X. \quad \text{(A.10)}$$

The same holds from the viewpoint of Z, namely,

$$\Delta\mathrm{MCR}(Z \,|\, X)_Y < \Delta\mathrm{MCR}(Z \,|\, Y)_X. \quad \text{(A.11)}$$

Figure 8 shows the numerical results.

(c) X is a common response [Fig. 1(c)].
When X is the common receiver, Y and Z are independent of each other. Hence, we derive the same theoretical results as the case that X is the common driver. Particularly, we have

$$\Delta\mathrm{MCR}(X \,|\, Y)_Z = \Delta\mathrm{MCR}(X \,|\, Z)_Y, \quad \text{(A.12)}$$

$$\Delta\mathrm{MCR}(Y \,|\, X)_Z < \Delta\mathrm{MCR}(Y \,|\, Z)_X, \quad \text{(A.13)}$$

$$\Delta\mathrm{MCR}(Z \,|\, X)_Y < \Delta\mathrm{MCR}(Z \,|\, Y)_X. \quad \text{(A.14)}$$

Figure 9 shows the numerical results.

(d) Z indirectly coupled with X, but directly driven by Y [Fig. 1(d)].
Because of the asymmetry of $\mathrm{MCR}(Y \,|\, X)$ and $\mathrm{MCR}(X \,|\, Y)$, one expects the difference

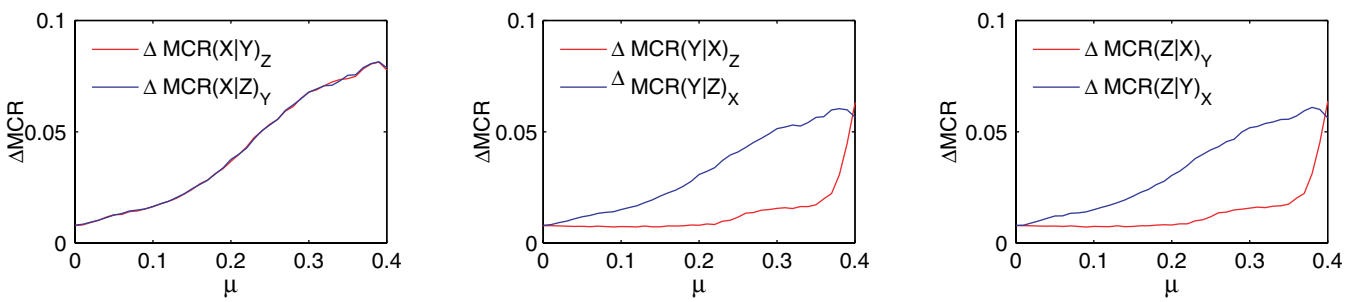

(a) (b) (c)

Fig. 8. X is the common driver for both Y and Z [Fig. 1(b), $\mu_{12} = \mu_{13} = \mu$, $\mu_{ij} = 0$ otherwise]. (b) From X viewpoint, $\Delta\mathrm{MCR}(Y \,|\, X)_Z < \Delta\mathrm{MCR}(Y \,|\, Z)_X$, [Eq. (A.10)]. (c) The same holds for (Eq. (A.11)), verified by $\Delta\mathrm{MCR}(Z \,|\, X)_Y < \Delta\mathrm{MCR}(Z \,|\, Y)_X$. Note that when $\mu > 0.39$, Y is synchronized with X suggested by the Lyapunov exponent spectrum (not shown in this paper).

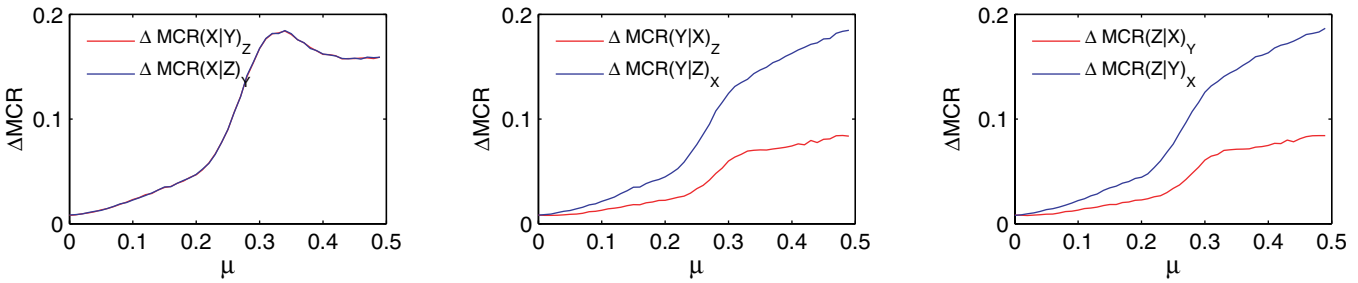

(a) (b) (c)

Fig. 9. X is the common receiver for both Y and Z [Fig. 1(c), $\mu_{21} = \mu_{31} = \mu$, $\mu_{ij} = 0$ otherwise]. Equations (A.12)–(A.14) are verified (see the caption of Fig. 8).

between $\Delta\mathrm{MCR}(Y\,|\,X)_Z$ and $\Delta\mathrm{MCR}(X\,|\,Y)_Z$. More specifically, the values of Eqs. (16)–(21) are not zero.

Note that within the coupling setting [Fig. 1(d)], we have $\langle p(\mathbf{x}_j)\rangle > \langle p(\mathbf{y}_j)\rangle > \langle p(\mathbf{z}_j)\rangle$. Before synchronization (neither two subsystems are synchronized), $\langle p(\mathbf{x}_j)\rangle > \langle p(\mathbf{y}_j, \mathbf{z}_j)\rangle$, $\langle p(\mathbf{y}_j)\rangle > \langle p(\mathbf{x}_j, \mathbf{z}_j)\rangle$, and $\langle p(\mathbf{z}_j)\rangle > \langle p(\mathbf{x}_j, \mathbf{y}_j)\rangle$. Furthermore, the complexity of (X, Z) is greater than the complexity of the joint space of (Y, Z). This leads to the joint recurrence probability of $\langle p(\mathbf{y}_j, \mathbf{z}_j)\rangle$ being greater than $\langle p(\mathbf{x}_j, \mathbf{z}_j)\rangle$. Hence we have $\mathrm{MCR}(Z\,|\,Y) > \mathrm{MCR}(Z\,|\,X)$, which yields

$$\Delta\mathrm{MCR}(Z\,|\,Y)_X < \Delta\mathrm{MCR}(Z\,|\,X)_Y. \quad \text{(A.15)}$$

From the viewpoint of Z, the relationship of the inequality of (A.15) suggests that the contribution of indirect coupling from X to Z is smaller than that of the direct coupling from Y to Z. This is validated by showing a similar relationship from the X perspective, namely,

$$\Delta\mathrm{MCR}(X\,|\,Y)_Z < \Delta\mathrm{MCR}(X\,|\,Z)_Y. \quad \text{(A.16)}$$

However from the mediator Y viewpoint, it sends out the coupling information to Z when receiving the same amount of information from X. Hence, one has

$$\Delta\mathrm{MCR}(Y\,|\,X)_Z \lessapprox \Delta\mathrm{MCR}(Y\,|\,Z)_X, \quad \text{(A.17)}$$

indicating Y to be the mediator. Figure 10 shows the numerical results.

(e) Direct coupling setting: X is the common driver and Z is the common receiver [Fig. 1(e)]. From the perspective of system X, both Y and Z have the same contribution to X, namely, we have

$$\Delta\mathrm{MCR}(X\,|\,Z)_Y < \Delta\mathrm{MCR}(X\,|\,Y)_Z. \quad \text{(A.18)}$$

From the viewpoint of Z, it accepts two packages of information from the driver X. One is from the direct contribution sent by X to Z; the other is received via the mediator Y. Z cannot distinguish where these two packages of information come from. Therefore, we have

$$\Delta\mathrm{MCR}(Z\,|\,X)_Y < \Delta\mathrm{MCR}(Z\,|\,Y)_X, \quad \text{(A.19)}$$

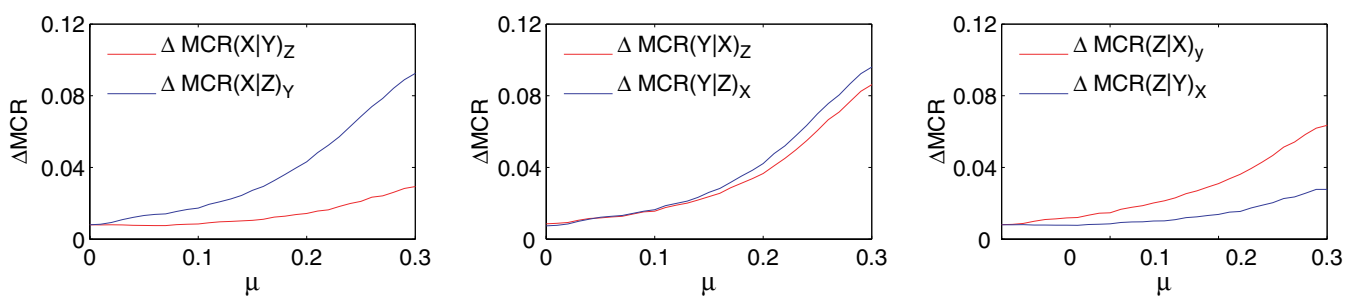

(a) (b) (c)

Fig. 10. X drives Y, and Y drives Z [Fig. 1(d), $\mu_{12} = \mu_{23} = \mu$, $\mu_{ij} = 0$ otherwise]. (a) $\Delta\mathrm{MCR}(X\,|\,Y)_Z < \Delta\mathrm{MCR}(X\,|\,Z)_Y$, (c) $\Delta\mathrm{MCR}(Z\,|\,Y)_X < \Delta\mathrm{MCR}(Z\,|\,X)_Y$. (b) However, Y is a mediator, having $\Delta\mathrm{MCR}(Y\,|\,X)_Z \lessapprox \Delta\mathrm{MCR}(Y\,|\,Z)_X$.

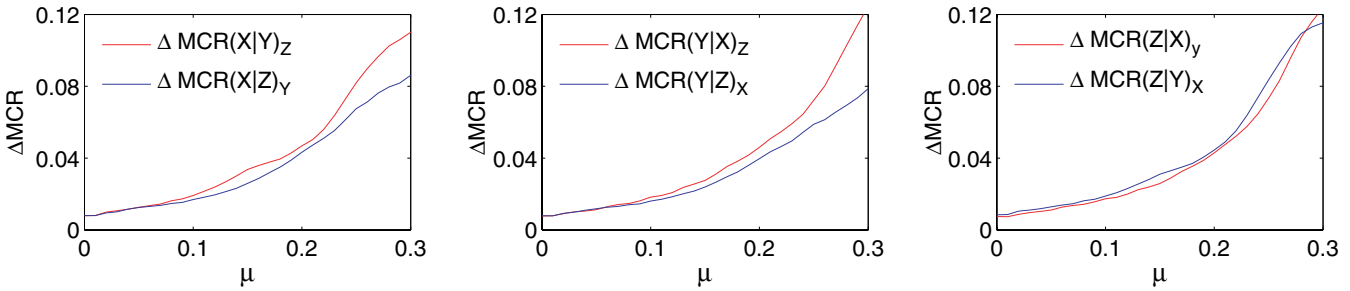

(a) (b) (c)

Fig. 11. X drives both Y and Z, and Y drives Z [Fig. 1(e), $\mu_{12} = \mu_{13} = \mu_{23} = \mu$, $\mu_{ij} = 0$ otherwise]. (a) $\Delta\mathrm{MCR}(X \,|\, Z)_Y < \Delta\mathrm{MCR}(X \,|\, Y)_Z$. (b) $\Delta\mathrm{MCR}(Y \,|\, Z)_X < \Delta\mathrm{MCR}(Y \,|\, X)_Z$ holds before synchronization. (c) $\Delta(Z \,|\, X)_Y < \Delta(Z \,|\, Y)_X$.

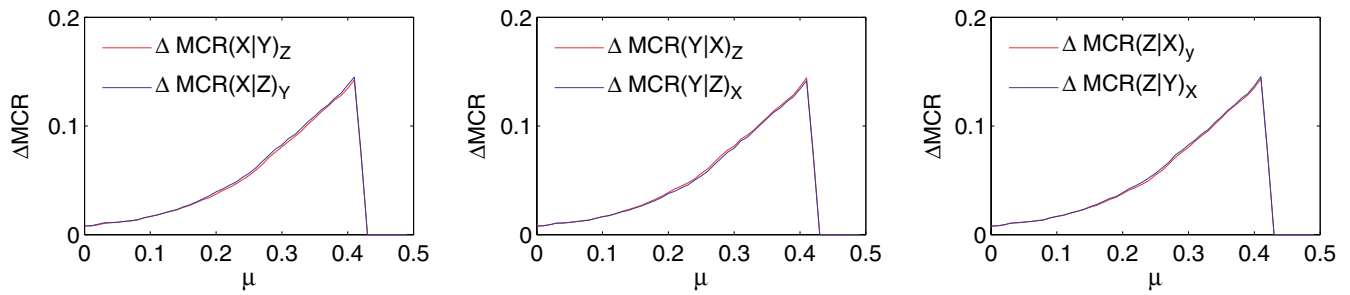

(a) (b) (c)

Fig. 12. X drives Y, Y drives Z, and Z drives X [Fig. 1(f), $\mu_{12} = \mu_{23} = \mu_{31} = \mu$, $\mu_{ij} = 0$ otherwise] [Eqs. (A.21)–(A.23)].

indicating that the transitivity property of Y is identified. Before onset of synchronization, we again have $\langle p(\mathbf{x}_j)\rangle > \langle p(\mathbf{y}_j)\rangle > \langle p(\mathbf{z}_j)\rangle$. Further, the relationship of $\langle p(\mathbf{x}_j, \mathbf{y}_j)\rangle > \langle p(\mathbf{y}_j, \mathbf{z}_j)\rangle$ holds. Hence, from the viewpoint of Y, we have

$$\Delta\mathrm{MCR}(Y \,|\, Z)_X < \Delta\mathrm{MCR}(Y \,|\, X)_Z. \quad \text{(A.20)}$$

Figure 11 shows the numerical results.

(f) Direct coupling setting: in a ring way [Fig. 1(f)]. All measures are the same, since each system shows basically the same recurrence behavior, namely,

$$\Delta\mathrm{MCR}(X \,|\, Y)_Z = \Delta\mathrm{MCR}(X \,|\, Z)_Y, \quad \text{(A.21)}$$

$$\Delta\mathrm{MCR}(Y \,|\, X)_Z = \Delta\mathrm{MCR}(Y \,|\, Z)_X, \quad \text{(A.22)}$$

$$\Delta\mathrm{MCR}(Z \,|\, X)_Y = \Delta\mathrm{MCR}(Z \,|\, Y)_X. \quad \text{(A.23)}$$

Note that this only holds in the case when the three systems are identical, yielding the same transitivity ability. Figure 12 shows the numerical results.